# Enhanced photoelectrochemical detection of an analyte triggered by its concentration by a singlet oxygen-generating fluoro photosensitizer

# Enhanced photoelectrochemical detection of an analyte triggered by its concentration by a singlet-oxygen generating fluoro photosensitizer

Adrian Blidar[1,2], Stanislav Trashin[1], Erik N. Carrión[3], Sergiu M. Gorun[3], Cecilia Cristea[2], Karolien De Wael[1*]

[1]AXES Research Group, University of Antwerp, Groenenborgerlaan 171, 2010 Antwerp, Belgium

[2]"Iuliu Haţieganu" University of Medicine and Pharmacy, Department of Analytical Chemistry, 4 Pasteur St., 400349, Cluj-Napoca, Romania

[3]Department of Chemistry and Biochemistry and the Center for Functional Materials, Seton Hall University, New Jersey, 07079, USA

*KEYWORDS: singlet oxygen, rifampicin, antibiotic, photocatalysis, phthalocyanine.*

**ABSTRACT:** The use of a photocatalyst (photosensitizer) which produces singlet oxygen, instead of enzymes for oxidizing analytes creates opportunities for cost-efficient and sensitive photoelectrochemical sensors. We report that perfluoroisopropyl-substituted zinc phthalocyanine ($F_{64}$PcZn) interacts specifically with a complex phenolic compound, the antibiotic rifampicin (RIF), but not with hydroquinone (HQ) or another complex phenolic compound, the antibiotic doxycycline. The specificity is imparted by the preconcentration of RIF in the photocatalytic layer, as revealed by electrochemical and optical measurements, complemented by molecular modeling that confirms the important role of a hydrophobic cavity formed by the iso-perfluoroisopropyl groups of the photocatalyst. The preconcentration effect favorably enhances the RIF photoelectrochemical detection to nanomolar (ppb) concentrations, LOD = 7 nM (6 ppb) and the sensitivity to 2.8 $A \cdot M^{-1} \cdot cm^{-2}$. The selectivity to RIF, retained in the photosensitizer layer is further enhanced by the selective removal of all unretained phenols via a simple washing of the electrodes with pure buffer. The utility of the sensor for analyzing municipal wastewater was demonstrated. This, first demonstration of enhanced selectivity and sensitivity due to intrinsic interactions of a molecular photocatalyst (photosensitizer) with an analyte, without use of a biorecognition element may allow the design of related, robust, simple and viable sensors.

The use of enzymatic catalysis in electrochemical detection of phenols is well known.[1–3] However, enzymes-based sensors have limitations due to thermal and chemical instability of enzymes, relative short shelf life of component biomolecules and limited reproducibility of enzymatic activity in using different biocatalyst batches.[4,5]

We have recently introduced a new, bioinspired detection strategy and have demonstrated it for the detection of phenols. Specifically, we have replaced a biological oxidation catalyst, Horse radish peroxidase (HRP) that uses $H_2O_2$ to oxidize phenols, with a heme-like photosensitizer that photo generates singlet-oxygen, $^1O_2$, using air under visible light illumination.[6] The photosensitizer, a zinc complex belonging to the class perfluoroalkyl-substituted perfluoro phthalocyanines,[6] lacks C-H bonds and thus exhibits high thermal and chemical robustness, thereby overcoming the shortcomings of the enzymatic biosensors. The photodynamic effect, Type II mechanism of generating singlet-oxygen is efficient and leads to high detection sensitivity.[6,8]

While the photosensitizer catalyzes the oxidation of phenols by oxygen, thus, mimicking the reactivity pathway of a biocatalyst (e.g., peroxidase or phenol oxidase) in biosensors[1–3], its molecular mechanism is different, namely an initial [4+2] cycloaddition of $^1O_2$ followed by the formation of the corresponding quinone.[7] The quinone is then electrochemically reduced under mild conditions back to a phenol (e.g., hydroquinone (HQ) or its derivative) thus completing the electrocatalytic cycle[8] similar to the action of peroxidases.[3] Importantly, the photocatalytic response occurs only under illumination, allowing the detection and quantification of the baseline in the presence of an analyte by simply switching the light off.[8]

Although the new method does not have an intrinsic specificity (in contrast to biosensors), a limited selectivity can be reached based on the differences in the oxygenation kinetics by $^1O_2$ for different phenols at different pH values.[8,9] For example, the highest photocurrent responses were obtained for HQ and p-aminophenol at neutral pH, in agreement with their fast oxidation kinetics. Under the same conditions, signal intensities obtained from more complex compounds containing a phenolic moiety, such as antibiotics amoxicillin and cefadroxil, were three times lower.[8,9] Other multifunctional phenolic compounds tend

to show even lower responses, likely due to steric hindrance and slow diffusion in solution and through the layer of the supported photocatalyst casted onto an electrode surface.

The enhanced selectivity and sensitivity of detection of phenolic analytes could be based on their interactions with the photosensitizer or its supporting matrix e.g., $TiO_2$ or $SiO_2$. The interaction of $TiO_2$ surface with the vicinal phenols 1,2-dihydroxybenzene and 1,8-dihydroxynaphthalene has been reported.[10,11] In our case, the photosensitizer $F_{64}$PcZn exhibits a strong Lewis acidic, hydrophilic metal center and a highly hydrophobic ligand cavity, both opposite features being simultaneously imparted by the fluorine substituents: the higher the number of fluorine groups, especially aliphatic ones, the more hydrophobic the ligand is, but also the more electron withdrawing, thus enhancing the metal electron deficiency and, consequently, its affinity for functional groups bearing electronic lone pairs. Indeed, single-crystal X-ray structures of $F_{64}$PcM complexes, M = Zn, Co, V=O, have revealed the presence of axial N and O atoms coordination, including the O of $H_2O$.[6] The hydrophilic Zn center may thus contribute to the binding of an analyte via coordination bonds, in addition to van der Waals (vdW) interactions, the latter being observed for non-sterically hindered phthalocyanine materials that adsorb polycyclic aromatic rings.[12,13] The role of supported photosensitizers in photochemically-induced electrosensing is complex. The layer of the supported photosensitizer is not electrically conductive, the photocurrent response measured by the sensor being the result, *inter alia*, of a complex interplay of the adsorption/desorption kinetics and diffusion of the analyte. Despite this complexity, the interactions between an analyte and the supported photosensitizer could be a viable, rational approach for improving the detectability of complex phenolic compounds, for example the antibiotic rifampicin (RIF).

The rise of antibiotic resistance, including towards RIF has become a worrying problem for public healthcare,[14,15] as resistant bacteria can be induced in the environment under selection pressures of antibiotics present in effluents and the environment.[16] Thus, monitoring potentially contaminated effluents and wastewaters is essential to estimates levels of antibiotics discharged in the environment.[16–18] In particular, RIF, introduced for human use in 1960s remains alongside isoniazid an essential first-line antitubercular drug worldwide.[15]

We report here that molecular interactions between the supported $F_{64}$PcZn photosensitizer deposited on an electrode and RIF result in the selective preconcentration of the latter at the electrode, greatly enhancing the sensitivity of the photoelectrochemical sensor towards RIF. The preconcentration is selective, as it was not observed for simple phenols such as hydroquinone (HQ) or catechol (CTH) and more complex OH-reach phenols such as antibiotics doxycycline (DXC) and oxytetracycline (OTC).

To the best of our knowledge this is the first demonstration of an enhanced selectivity and sensitivity of a $^1O_2$-based photocatalytic sensor, which is ascribed to intrinsic interactions of the photocatalyst with an analyte, without the use of any biorecognition element.

## Experimental

**Materials**. The perfluorinated phthalocyanine zinc complex $F_{64}$PcZn was synthesized and deposited on $TiO_2$ (Degussa, P25) as described previously[19] resulting in the supported photosensitizer abbreviated $F_{64}$PcZn∪$TiO_2$. HQ, CTH and resorcinol (RES) were purchased from Sigma-Aldrich (Belgium). RIF (>95% purity), DXC (98% purity), and OTC (>95% purity) were purchased from Across Organics. The measuring buffer (phosphate buffer pH 6) consisted of 0.1 M KCl and 20 mM $KH_2PO_4$ dissolved in ultrapure water (18.2 MΩ, Millipore Simplicity) and adjusted to pH 6. Measuring buffers with a different pH or ionic strength are specified in the text.

**Instruments.** The photoelectrochemical measurements were conducted using a PalmSens2 potentiostat from Palmsens BV (Utrecht, The Netherlands) and a red 655 nm diode laser (Roithner Lasertechnik) operating at 30 mW power and adjusted to a spot diameter of 4 mm. A power supply (Arduino Uno) was used to switch on and off the light beam at preprogramed times. An AvaSpec-2048L UV-Vis spectrophotometer from Avantes (Netherlands) equipped with an AvaLight-DH-S-BAL light source was used for spectrophotometric measurements.

**Electrodes.** Screen-printed electrodes (SPE, DRP-110, DropSens, Spain) with carbon working area of 4 mm in diameter were typically, unless stated otherwise, modified by depositing a single 5 µl droplet of an aqueous suspension of 10 mg/ml $F_{64}$PcZn∪$TiO_2$ (3% wt.) followed by overnight drying. The modified electrodes are abbreviated $F_{64}$PcZn∪$TiO_2$|SPE. Both the volume and concentration of $F_{64}$PcZn∪$TiO_2$ suspensions were varied in order to optimize the amount of deposited materials.

Prior to photoelectrochemical measurements, 80 µl of a RIF solution was placed on $F_{64}$PcZn∪$TiO_2$|SPE and the electrodes where kept in the dark in a closed vessel. Chronoamperometric measurements were carried out using either a drop of the same RIF solution or pure buffer (after additional rinsing with pure buffer). For experiments involving sequential illuminations lasting a total of 4 hours the drop was refreshed after each illumination. For the hydrodynamic setup, four $F_{64}$PcZn∪$TiO_2$|SPE were immersed in 16 ml of RIF solution and stirred magnetically at 300 rpm for 2 hours. Following the bulk equilibration, the electrodes were removed from the solution, connected to a potentiostat and covered by a single drop of the same RIF solution.

**UV-Vis quantification of RIF adsorbed on solid $TiO_2$ and $F_{64}$PcZn∪$TiO_2$.** 1, 2, 3 or 4 mg of solid $TiO_2$ or $F_{64}$PcZn∪$TiO_2$ were weighed in Eppendorf tubes, washed 3x with phosphate buffer pH 6 using a vortex and an ultrasonic bath for resuspension (for 10 min) and then centrifuged at 7000 rpm (for 5 min) to isolate the powders. Finally, the powders were resuspended in 1 ml of 10 µM RIF solution in phosphate buffer pH 6 and left in dark for 2 hours on a mechanical agitator. Afterwards, the suspensions were centrifuged at 14000 rpm for 30 min to remove all solid particles and UV-Vis spectra of the supernatants were recorded using a 0.5 cm a quartz cell to assess the change in the RIF concentration from the initial 10 µM.

**Molecular modeling of RIF-$F_n$PcZn interactions.** The docking of RIF onto $F_n$PcZn were performed using the *GOLD v. 2020.1* program[20], RIF was designated as the "ligand" while $F_n$PcZn were the "protein". RIF conformers were initially generated via *Mercury CSD Conformer Generator v. 2020.*[21] to minimize conformational biases during docking calculations. A coordination binding site with a 10 Å radial distances from the Zn center was selected given the likely propensity of RIF oxygen-based functional groups for binding to the electron deficient metal. Docked RIF-PcZn structures were visualized with *Hermes v. 2020.1*.[21] A fine grid of fitting points, keeping the vdW interaction energies below -2.5 kcal/mol was incorporated at the binding site to illustrate *van der Waals* interactions between $F_n$PcZn and RIF. Additional dockings were performed using Zn-O bond distance constraints of approximately 2.1, 2.3, and 2.5 Å consistent with statistical data on zinc-oxygen interactions, Figure S2.

Rough RIF-$F_n$PcZn enthalpic interaction energies were obtained using *MOPAC2016* with the PM7 Hamiltonian. Geometry minimizations were performed until potential energy gradients were <10 kcal/mol/Å for RIF complexes and <1 kcal/mol/Å for $F_n$PcZn. A dielectric constant, ε = 78.4 was introduced to mimic the aqueous environment in phosphate buffer saline.

**Municipal wastewater analysis.** Samples of effluents obtained from the Cluj-Napoca Wastewater Treatment Plant (Cluj, Romania) were spiked with a solution of RIF in phosphate buffer pH 6 and passed through a 0.45 µm pore size membrane filter (Chromafil AO-45/25, Macherey-Nagel, Germany) to give a final RIF concentration of 1 µM. Samples were diluted 10 times with the measuring buffer before being analysed.

## Results and discussion

**Photoelectrochemical detection of RIF**. The molecular structures of studied compounds exhibiting at least one phenol group are shown in Figure 1. RIF, a zwitterion at physiological pH contains three phenolic hydroxyls grafted on its naphthalene core structure. Two of them, at positions 1 and 4 form a hydroquinone-like moiety. The third one, position 8, is deprotonated while a piperazine N is protonated ($pK_a$ = 3, $pK_b$ = 7.5).[22,23] RIF is slowly oxidized by oxygen in aqueous solutions to form rifampicin quinone RIF-Q (within hours at pH 7.5 and 37° C).[24]

The $^1O_2$-based photoelectrochemical detection of phenols, including RIF is shown in Figure 2A. The detection of RIF (or HQ) relies on two main processes: (1) the oxidation of RIF by $^1O_2$ that is generated by $F_{64}$PcZn under illumination from air oxygen, and (2) the electrochemical reduction at an electrode of a formed product or products. These two processes create the redox cycling that enhances sensitivity of the detection method.[6]

The method has been proven to work for antibiotics containing a phenolic moiety such as amoxicillin, cefadroxil and doxycycline.[8,9] RIF contains a hydroquinone (HQ) moiety that can be reversibly oxidized into the corresponding quinone RIF ↔ RIF-Q, Figure 2A. Thus, RIF is expected to be well-detectable via oxidation with $^1O_2$. The zwitterionic and oxidized forms of RIF, however, are large molecules with multiple functionalities and charges that may interact with $F_{64}$PcZn∪$TiO_2$ and the electrode material (carbon ink) complicating the detection. Indeed, the profile of the amperometric response drastically differs for RIF in comparison with HQ, Figure 2B. In the first few seconds after the light triggered the response, the photocurrent was similar for both HQ and RIF, but decayed for RIF while remaining constant for HQ. The steady-state photocurrent for RIF was reached in about 10 min resulting in a four times lower value compared to the steady-state current for HQ.

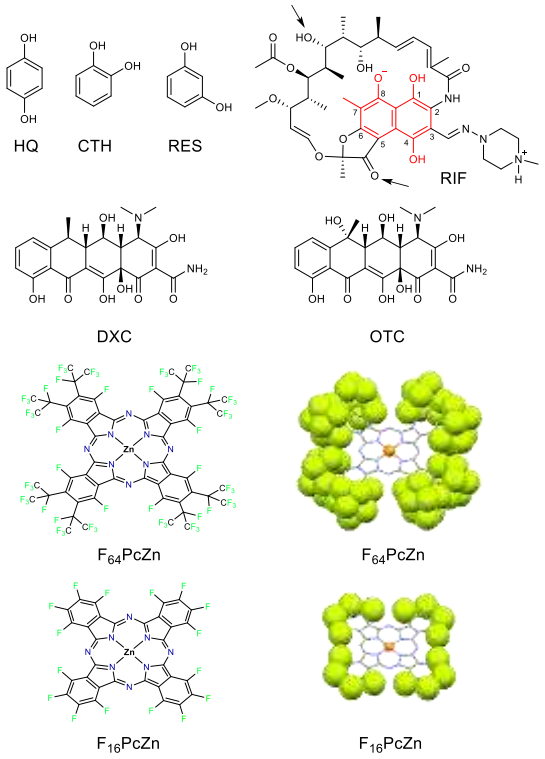


**Figure 1.** Molecular structures of studied compounds with at least one phenol group and the FnPcZn phthalocyanines, n = 16, 64. The F atoms are depicted as vdW spheres. The Zn is represented as a small sphere; the remaining atoms are depicted as capped sticks. Color code: Zn, orange; F, green; C, gray; N, blue. The arrows point toward the –OH and =O groups found via dockings to be closest to the Zn centers of $F_{16}$PcZn and $F_{64}$PcZn, respectively. See also Figures S3 and S4.

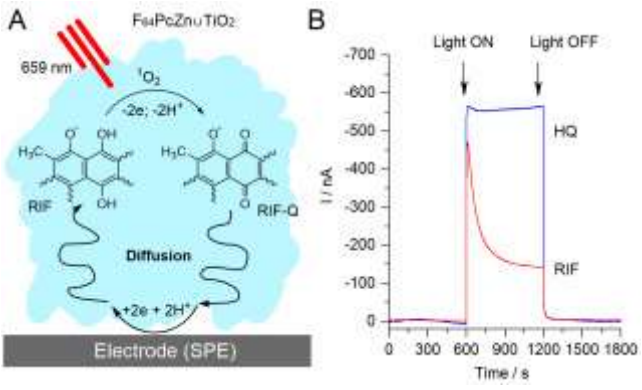


**Figure 2.** (A) Schematic representation of the mechanism for the photocurrent response of RIF using the $F_{64}$PcZn∪$TiO_2$|SPE electrode. (B) A typical photoelectrochemical response at −0.1 V potential of 10 µM HQ (blue) and 10 µM RIF (red) in phosphate buffer pH 6.

The shape of the current response as a function of time suggests that RIF and RIF-Q may exhibit poor diffusion in the $F_{64}PcZn \cup TiO_2$ layer, leading to the corresponding decay of the photocurrent measured by $F_{64}PcZn \cup TiO_2$|SPE. The slow diffusion may result in slow equilibration of the electrode in the RIF solution, a hypothesis that was examined by using longer equilibration times combined with (1) multiple short illuminations, or (2) a single illumination at the end of the long equilibration time, Figure 3. Considering the significant decay of the signal, Figure 2B, the illumination time was shortened to 10 s.

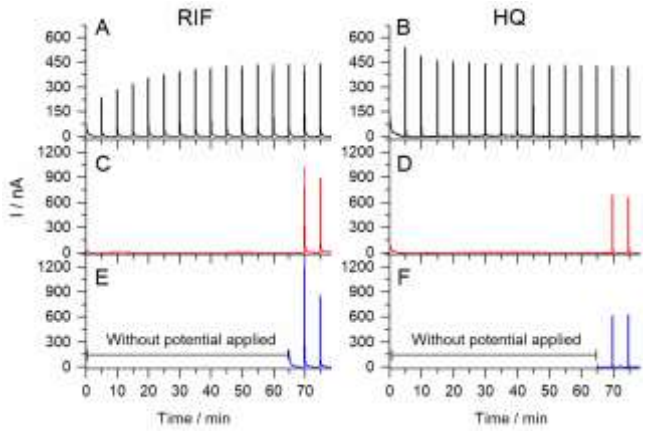


**Figure 3.** Photoelectrochemical measurements of 10 μM RIF (A, C, E) and 10 μM HQ (B, D, F) in phosphate buffer pH 6 using a series of cycles of dark (290 s) and light (10 s) periods (A, B); a long preconditioning in dark for 70 min followed by a short illumination for 10 s at a continuously polarized electrode (C, D); and a long equilibration step (65 min) of a disconnected electrode followed by a measurement with a short illumination time of 10 s (E and F). Potential applied, −0.1 V. Coating, 4 μg/mm$^2$.

Sequential illumination/dark cycles, 10/290s, Figure 3A revealed that the photocurrent for RIF increased 1.8 times during first 10 – 12 illumination/dark periods and stabilized afterwards, i.e. after about 1 hour. In contrast, the HQ photocurrent showed a small decrease by 17% using the same illumination protocol during the first 5 – 6 periods, Figure 3B, reaching after about 30 minutes a stable value identical to the response of RIF.

Surprisingly, an extended equilibration step without illumination, about 70 min, similar to the time of the first 12 dark/illumination periods (60 min) resulted in a further enhancement of the photocurrent for RIF, Figure 3C, compared with both the response after 5 and 60 min, Figure 3A. Under prolonged equilibration, the photocurrent response for RIF, Figure 3C, was even higher than that for HQ, Figure 3D. Moreover, the equilibration step was more efficient for RIF even without the potential applied, compare Figure 3C and 3E. To conclude, the photocurrent response for RIF (−1.2 μA) was 2x the response of HQ (−0.62 μA) obtained after equilibration of disconnected electrodes in RIF or HQ solutions, respectively, while the response of RIF after the equilibration was 5x the response of RIF without the equilibration step (the first illumination in Figure 3A).

Taken together, RIF can be preconcentrated at the surface of the modified electrode during the equilibration period, resulting in an enhanced sensitivity to RIF in solution compared with HQ. Given the above, a protocol that includes the preconcentration step of RIF without electrode polarization was employed. This protocol insured that the highest response was obtained and allowed the simultaneous equilibration of several electrodes.

**Kinetics of RIF preconcentration on $F_{64}PcZn \cup TiO_2$|SPE.** The diffusion of RIF is slow and thus the saturation of the interfacial $F_{64}PcZn \cup TiO_2$ layer may require hours. Hence, the maximum current response depends on the initial concentration of RIF in solution and the thickness of the $F_{64}PcZn \cup TiO_2$ layer on the electrode. The general picture of RIF accumulation kinetics was obtained using a batch of electrodes incubated separately for a given time in RIF solution. For the first 120 min a near constant photocurrent was measured for HQ, whereas for RIF a steep increase in the photocurrent, that reached −1200 nA, was observed, Figure 4A. Decreases, up to 30% were observed after additional 120 min, attributed to the worsening of adhesion of the $F_{64}PcZn \cup TiO_2$ coating with time, and, thus, its mechanical instability during electrode manipulations.

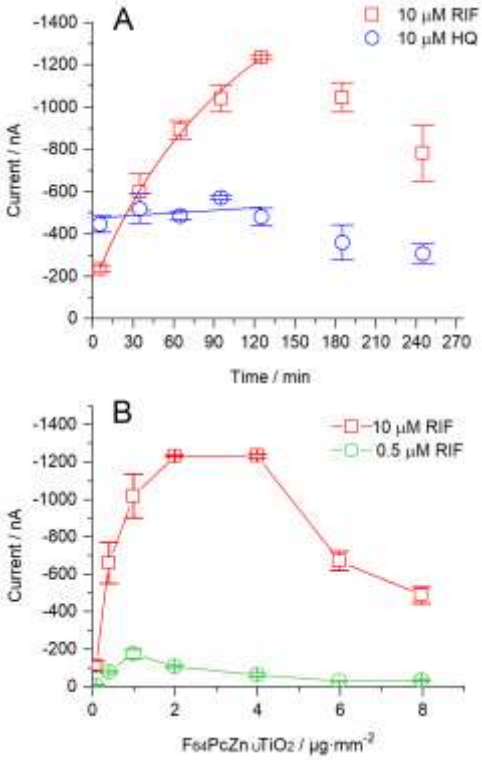


**Figure 4.** (A) The photoelectrochemical response to 10 μM RIF (red) and 10 μM HQ (blue) as a function of incubation time. (B) Effect of $F_{64}PcZn \cup TiO_2$ coverage (layer thickness) on the photoelectrochemical response after 2 h incubation in 10 and 0.5 μM RIF. Each data point was measured using three separate electrodes incubated individually in a drop of RIF or HQ solution for a given time. The error bars equal the standard deviations.

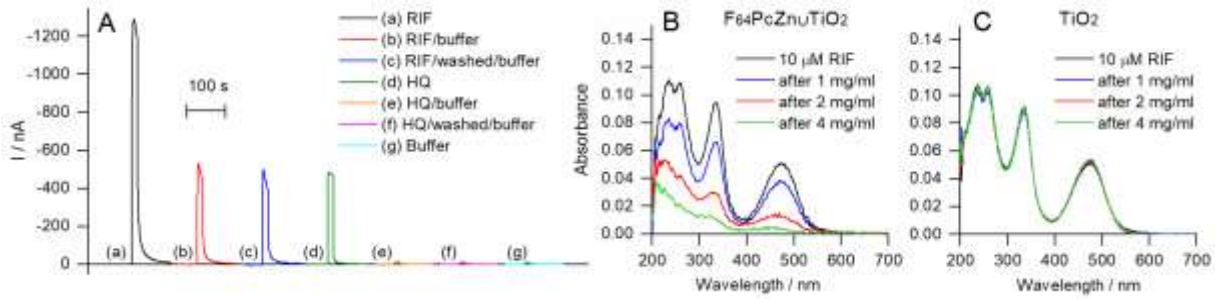


**Figure 5.** Photoelectrochemical responses (A) of 10 μM RIF (a-c), 10 μM HQ (d-f) and blank buffer (g) obtained after 2 h incubation in the respective solution followed by either testing using the same solution (a, d) or washing and testing in blank buffer (b, c, e, f). Other conditions are the same as those in Figure 3. The UV-Vis spectra of the RIF solution after incubation with different amounts of $F_{64}PcZn \cup TiO_2$ (B) and $TiO_2$ (C).

The effect of $F_{64}PcZn \cup TiO_2$ coating amount was examined next. A set of electrodes with coatings ranging from 0.08 to 8 μg/mm² preequilibrated in RIF solution for 120 min were tested, Figure 4B. For 10 μM RIF concentration, the current increases roughly proportionally up to 2 μg/mm² when the entire electrode seems to be coated, see Figure S1A. Then the current intensity drops with increase loading reaching 50% of its maximum value at 8 μg/mm². This can be explained by accumulation of RIF in the upper part of the layer which slows equilibration of $F_{64}PcZn \cup TiO_2$ in the part of the layer close to the electrode. This additionally confirmed by decrease in gradient of the time-dependent signal with the amount of $F_{64}PcZn \cup TiO_2$, Figure S1B.

Interestingly, the effect of the layer thickness was much more pronounced for 0.5 μM RIF with the maximum photocurrent at 1 μg/mm² (in contrast to 2–4 μg/mm² for 10 μM RIF) followed by 5-fold drop in the response then the thickness of the layer increased 8 times (from 1 to 8 μg/mm²), Figure 4B. Thus, thinner coatings seemly improve the detection of RIF in the sub-micromolar concentration range by facilitating the saturation of the photosensitizer at close proximity to the electrode but may limit the sensitivity at higher concentrations due to saturation of the $F_{64}PcZn \cup TiO_2$ layer.

**RIF adsorption by $F_{64}PcZn \cup TiO_2$ and $F_{64}PcZn \cup TiO_2$|SPE**

The adsorption of RIF was probed by using electrodes preequilibrated in a solution of RIF, washed in pure buffer and then used for detection of the photocurrent. Figure 5 shows the responses of RIF and, for comparison, HQ, with and without washing with pure buffer. Following a single washing the initial signal, Figure 5A, trace (a) loses about 60% of its intensity, Figure 5A, trace (b) but this value remains constant at least after the 3rd washing, Figure 5A, trace (c). In contrast to RIF, the photocurrent response for HQ dropped to the level of blanks after washing with pure buffer as shown in Figure 5A, traces (d)-(g). These data indicate that even after rigorous washing RIF remained at the electrode, whereas HQ was easily and completely removed, thus suggesting that preconcentration imparts detection selectivity, simple phenols being prevented from interfering by washing. Further proof of RIF adsorption was obtained by measuring directly its concentration decrease in solution in the presence of $F_{64}PcZn \cup TiO_2$, Figure 5B. Following incubation of a 1 ml 10 μM RIF solution with 1 mg/ml suspension $F_{64}PcZn \cup TiO_2$, a composition roughly corresponding to conditions of amperometric analysis with $F_{64}PcZn \cup TiO_2$|SPE (50 μl drop of 10 μM RIF, 4 μg/mm² $F_{64}PcZn \cup TiO_2$ or 50 μg per electrode), a decrease in UV-Vis absorbance at 474 nm after 2 h incubation corresponding to loss of 27% of RIF was observed. Increasing the amount of $F_{64}PcZn \cup TiO_2$ fourfold resulted in the near complete removal of RIF from the solution. In average, 3.0 ± 0.6 nmol RIF are adsorbed on 1 mg $F_{64}PcZn \cup TiO_2$, which is comparatively large. A layer of 4 μg/mm² can create deficiency of RIF over 1 mm distance from $F_{64}PcZn \cup TiO_2$|SPE already for 10 μM RIF unstirred solution or even larger distances for more diluted RIF solutions, which correlates well with slow kinetics of RIF preconcentration.

Since $TiO_2$ alone does not absorb RIF, Figure 5C, the preconcentration of RIF by $F_{64}PcZn \cup TiO_2$|SPE is ascribed to the supported fluorinated photosensitizer, $F_{64}PcZn$. Theoretical modeling provides insights into this binding.

**Molecular modeling of RIF-$F_{64}PcZn$ interactions.** RIF, Figure 1, exhibits aromatic rings and N- and O-based functional groups that could contact the phthalocyanine scaffold via stacking, vdW or metal-coordination interactions. The absence of adsorption effects for HQ and 4-aminophenol[8] suggest that the interactions of amino- or phenol groups alone cannot explain the observed RIF-$F_{64}PcZn$ interactions. Notably, HQ and 4-aminophenol are relatively small and thus the coordination of their O and N groups to the Zn centers of phthalocyanines, Figure 1, is not sterically hindered. Aromatic stacking interactions are also not precluded for $F_{16}PcZn$, but they are for $F_{64}PcZn$ by the *iso*-perfluoro alkyl groups (*iso*-$R_f$). On the other hand, the bulky, peripheral *iso*-$R_f$ groups form a hydrophobic cavity around the metal raising the possibility of vdW interactions, including with RIF. Insights into the role of *iso*-$R_f$ groups, the structural chemistry of $F_{64}PcZn$ was compared with that of $F_{16}PcZn$, an electronically similar complex, but with all *iso* perfluoro alkyl groups replaced by aromatic F groups, Figure 1. The hydrophobic cavity is thus eliminated, rendering $F_{16}PcZn$ sterically unhindered. A histogram of the Zn-O bond length in $F_nPcZn$-O complexes, Figure S2, with the oxygen belonging to water, ether, ketone, alcohol, ester, amide, sulfoxide, phosphine oxide and nitrito functional groups revealed a quasi-Gaussian distribution. The PcZn-O distances vary between 1.949 and 2.178 Å, with a mean of 2.100(9) Å for the crystal structures with R < 15% reported in the Cambridge Structural

Database (CSD, 03/2020 update), with the notable exception of the $F_{64}$PcZn(acetone)$_2$ outlier, for which the Zn-O distance is 2.445 Å. Long bonds indicate weak binding and thus one would predict an unstable $F_{64}$PcZn(acetone) complex despite the enhanced Lewis acidity of the Zn imparted by the fluorine-rich ligand. Yet the complex has been stable in crystalline form for over a year in air, a fact that could be ascribed not only to the usual (unspecified) "solid-state effects", but, more specific, at least in part, to the vdW interactions of acetone with the fluorinated pocket in which it resides. The geometry of the optimized $F_{16}$PcZn-RIF and $F_{64}$PcZn-RIF complexes is shown in Figures 6 and S3 and S4. The keto group of RIF, marked with an arrow in Figure 1A is the closest to the metal center of $F_{64}$PcZn, Zn---O = 4.328 Å. A shorter distance, 3.466 Å is noted for the Zn---OH (aliphatic), $F_{16}$PcZn. Both distances are, however, at least ~50% longer than the Zn-O range mentioned above and thus the binding is extremely weak. Nevertheless, based only on Zn---O coordinative interactions RIF cannot be expected to have a much higher affinity $F_{64}$PcZn , but its stronger association with it is suggested by molecular mechanics based on its vdW interactions with the *iso*-$R_f$ groups, as also illustrated by the 2x more vdW fit points (radial coverage) for $F_{64}$PcZn-RIF relative to $F_{16}$PcZn-RIF, Figure S4.

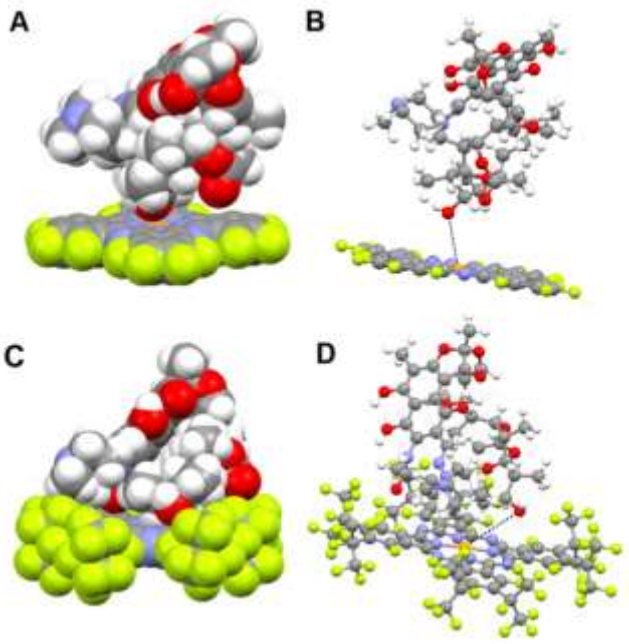


**Figure 6.** Geometry optimized complexes of $F_{16}$PcZn-RIF and $F_{64}$PcZn-RIF depicting all atoms as vdW sphere (A and C) and ball-and-stick (B and D) representations. Color code: Zn, orange, C, gray, F, green, N, blue, O, red. Measured Zn-O bond distances were 3.466 Å and 4.328 Å.

The zwitterionic form of RIF, Figure 1 was also modeled. This form is present in solution, but it is unlikely to exist in the absorbed RIF since the phenolic oxygen, position 8, cannot approach the Zn while the aliphatic OH is unlikely to ionize, while the ketone group does not, a keto-enol equilibrium notwithstanding. Consistent with this view, X-ray structures at 2.70 Å resolution of poxvirus-rifampicin complexes reveal that the antibiotic is in its neutral form.[25] The modeling indicates that the neutral and zwitterionic RIFs behave similarly with respect to binding $F_n$PcZn, viz. the binding to $F_{64}$PcZn over $F_{16}$PcZn is favorite, thus supporting the conclusions reached for the neutral form.

Consistent with the computed lack of significant variations of RIF-$F_{64}$PcZn∪$TiO_2$|SPE interactions, as well as with the lack of electrostatic-type interactions, whether RIF is a neutral molecule or a zwitterion, the photocurrent was found to be virtually independent of the ionic strength of the pH 6 phosphate, Figure S5. This observation is also consistent with predominant van der Waals type RIF-$F_{64}$PcZn∪$TiO_2$ interactions. Given the lack of ionic strength influence and in order to ensure reliable and reproducible conditions in further measurements, a standard phosphate buffer containing 20 mM phosphate and 100 mM KCl was used in all experiments.

**Optimization of the detection protocol.** The applied potential, pH and the photosensitizer loading on $TiO_2$ were varied to determine optimal conditions for preconcentration and detection of RIF. In particular, the working potential defines the kinetics of the electrochemical reduction of RIF-Q and should be optimized to ensure the maximal possible response at an acceptably low background current. The potential was varied from +0.10 V to −0.20 V. As shown in Figure 7A, the photocurrent response of RIF reaches a maximum at −0.10 V, decreasing at −0.15 V and further at −0.2 V. Thus, for the efficient reduction of RIF-Q a potential of −0.10 V was chosen for all experiments. This choice is consistent with our previous studies on other phenolic compounds in similar conditions,[8,9] a relatively low overpotential improves the selectivity by preventing possible oxidation of interfering analytes. This is an important advantage over oxidative amperometric or voltammetric detections.[26,27]

We have establish previously for several phenols[9], that higher pH values increase significantly the photocurrent response due to an increase in the oxidation rate of deprotonated phenols by $^1O_2$. However, RIF is chemically unstable at pH above 8 and below 4.[28] Thus, we studied the photocurrent response in this pH range using phosphate, citrate and Tris buffers. As shown in Figure 7B, Tris slightly improves the detection at pH 7 and 8 but the currents were not higher than those observed for phosphate at pH 6. The photocurrent was optimal in phosphate buffer pH 6, which is close to the optimal pH for extraction of RIF into a dimethylpolysiloxane layer used in HPLC assisted by stir bar-sorptive extraction.[29] A decrease in the photocurrent at pH 7 and 8 drastically differs from our previous work with other phenolic analytes where the photocurrent increased at higher pH.[9] This difference is ascribed to better preconcentration and mobility of RIF at pH 6 in the $F_{64}$PcZn∪$TiO_2$ layer.

Figure 7C depicts the effect of $F_{64}$PcZn wt% loading on $TiO_2$ on the photocurrent response. The photocurrent increased linearly with the loading up to 2wt%, a value consistent with the 3wt% one needed for monolayer coverage on $TiO_2$ P25. Additional $F_{64}$PcZn layers on top of the layer in direct contact with the support may act as barriers, surface morphology modifier as well as optical light absorbers thus limiting the efficiency of the photooxidation reaction.

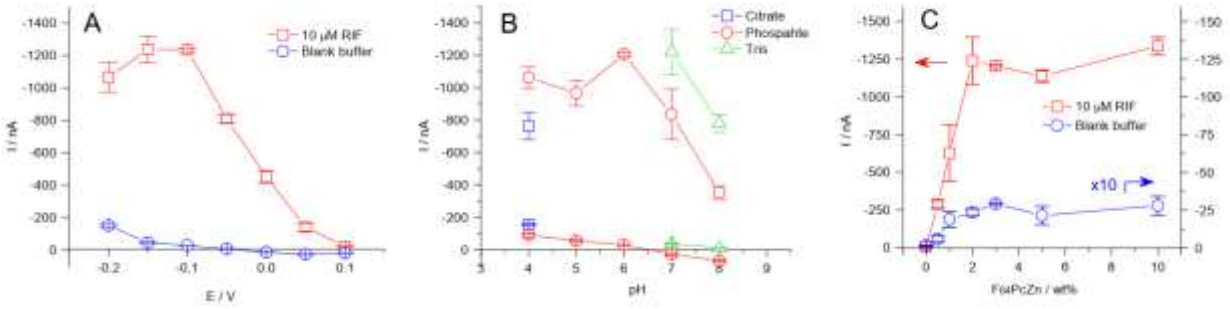


**Figure 7.** The influence of the potential (A), pH (B) and the $F_{64}PcZn$ loading in $TiO_2$ matrix (C) on the photocurrent response. Concentration of RIF, 10 mM; incubation time, 120 min. Other parameters are the same as in Figure 3. The error bars represent SD of three measurements.

**Analytical performance**. Taken together, the optimization studies led to the selection of 1 and 4 μg/mm² coatings for the construction of calibration curves. Figure 8A shows that the photocurrent response depended linearly on the concentration of RIF in range 0.05 - 2.5 μM and 0.1 - 10 μM for 1 and 4 μg/mm² $F_{64}PcZn \cup TiO_2$, respectively. Both ranges span about 2 orders of magnitude, but the one for the thicker coating was larger, congruent with the slow diffusion and accumulation of RIF. Conversely, the sensitivity in the low concentration range was more than three times higher for the thin layer, the slope being 348 nA·μM$^{-1}$ (2.77 A·M$^{-1}$·cm$^{-2}$) and 95.3 nA·μM$^{-1}$ (0.76 A·M$^{-1}$·cm$^{-2}$) for the 1 and 4 μg/mm² coverages, respectively.

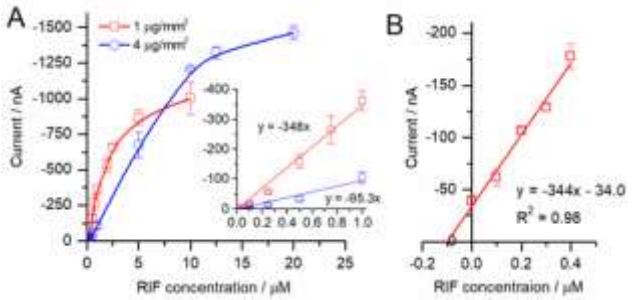


**Figure 8.** (A) Calibration plots for RIF obtained at electrodes coated with 1 and 4 μg/mm² $F_{64}PcZn \cup TiO_2$. (B) Analysis of an effluent spiked with RIF by the standard addition method using electrodes with 1 μg/mm² $F_{64}PcZn \cup TiO_2$. Each data point and error bars represent an average and SD of three individual sensors. The blank signal of pure buffer was subtracted from the measurements.

The corresponding ***l***imit ***o***f ***d***etection (LOD), equals 3 standard deviation of blanks divided by the slope of the calibration curve, LOD = 3·$SD_{blank}$/slope), are estimated to be 7 and 28 nM for 1 and 4 μg/mm² $F_{64}PcZn \cup TiO_2$ coatings, respectively. These values, however, are difficult to reach in practice due to the slow preconcentration diffusion of RIF in dilute solutions. The accumulations can be accelerated by stirring, leading to a lowering of the LOD from 28 to 10 nM, as illustrated in Figure S6.

Importantly, the reported analysis method is more sensitive than the spectrophotometric assay (LOD = 0.7 μM)[30] as well as chromatographic[31,32] or electrophoretic[33] methods coupled with a UV-detector (Table S1).

The reported method is also comparatively simple to set-up and use. Indeed, enhanced sensitivity techniques have been used for the electrochemical detection of antituberculous drugs, mainly by adsorptive stripping voltammetry and various electrode modifications,[26,27] including with metallic lead, graphene oxide, gold and silver nanoparticles, carbon dots, metal oxides, molecularly imprinted polypyrrole and cyclodextrines and various combinations thereof. Most of these materials increase the electrode surface area, preconcentrate the analyte and facilitate its oxidation resulting in LOD values from low nanomolar to micromolar range. In contrast, the reported electrode modification requires neither a complex architecture nor modification procedures and can be easily scaled up for mass production while exhibiting one of the lowest LOD demonstrated.

Finally, the practical applicability and validity of the proposed method was tested on a wastewater treatment effluent spiked with RIF. The standard addition method, Figure 8B, yields a 344 nA·μM$^{-1}$ slope identical to that obtained from the pure buffer, thus suggesting no interference of the effluent matrix. The 99 ± 6 % (RSD = 6.2%, n = 3) recovery value indicates the adequate accuracy and repeatability of the proposed method for real sample analysis.

Additional improvement in selectivity toward phenols that adsorbs in the layer of the photosensitizer can be envisaged due to the retention of the analyte in the layer under washing with pure buffer. Table 1 lists relative response of RIF in comparison to three simplest dihydroxybenzenes (HQ, CTH, RES) and DXC and OTC, two antibiotics bearing several functional groups, including a phenolic moiety. RIF exhibited the highest photocurrent, followed by HQ, CTH and DXC.

**Table 1.** Photocurrent responses of phenols after incubation of electrodes for 2 h in their 10 μM solutions. Average ± SD of three measurements.

| Analyte | Photocurrent / μA | |
|---|---|---|
| | Measured in tested solutions | Washed and measured in pure buffer |
| RIF | −1.210 ± 0.010 (100%) | −0.480 ± 0.020 (100%) |
| HQ | −0.454 ± 0.003 (38%) | −0.016 ± 0.002 (3%) |
| CTH | −0.280 ± 0.050 (23%) | −0.059 ± 0.017 (12%) |
| RES | −0.004 ± 0.007 (0%) | −0.004 ± 0.002 (1%) |
| DXC | −0.100 ± 0.005 (8%) | −0.017 ± 0.004 (4%) |
| OTC | −0.030± 0.001 (2%) | −0.003 ± 0.002 (1%) |

Remarkably, the washing step widened the gap between the photocurrent responses of RIF and the other compounds. Except for RIF, only CTH was noticeably retained at the electrode after the washings, although showing a 5x loss of signal. In general, the interference of dihydroxybenzenes and both tetracyclines was diminished after the washing step.

## Conclusions

We demonstrate for the first time that a functionalized molecular photocatalyst (photosensitizer type II) exhibits analyte selectivity in interacting with a complex phenolic compound, viz. the antibiotic RIF, while showing no significant interactions with HQ or another complex phenolic compound, the antibiotic DXC. Experimental and modeling studies suggest the appearance of a preconcentration effect in a comparatively thick electrically nonconductive layer, which results in a favorable LOD, 7 nM (6 ppb). The preconcentration of RIF, a phenolic analyte in a thick, electrically nonconductive layer at the electrode surface is effective despite of its strong adsorption, resulting in a complex interplay among the diffusion, adsorption/desorption kinetics and photocatalytic oxidation/electrochemical reduction. Thus, functionalizing a robust photocatalyst and a supporting material with the aim of preconcentration of an analyte is an attractive strategy to fabricate cost-effective and ultrasensitive photoelectrochemical sensors.

## ASSOCIATED CONTENT

**Supporting Information**. All materials, reagents, instruments, experimental methods used in this study and more information are described in detail in the Supporting Information.

## AUTHOR INFORMATION

### Corresponding Author

* Karolien De Wael
e-mail: karolien.dewael@uantwerpen.be

### Author Contributions

All authors have approved the manuscript.

## ACKNOWLEDGEMENTS

This work was supported by ERA.Net RUS Plus Plasmon Electrolight project (No. 18-53-76006 ERA, Belgium) and the Center for Functional Materials, Seton Hall University (USA) This paper was published under the frame of European Social Found, Human Capital Operational Programme 2014-2020, project no. POCU/380/6/13/125171.

## REFERENCES

1. Imabayashi, S. I.; Kong, Y. T.; Watanabe, M. Amperometric Biosensor for Polyphenol Based on Horseradish Peroxidase Immobilized on Gold Electrodes. *Electroanalysis* **2001**, *13* (5), 408–412.
2. Yang, S.; Chen, Z.; Jin, X.; Lin, X. HRP Biosensor Based on Sugar-Lectin Biospecific Interactions for the Determination of Phenolic Compounds. *Electrochim. Acta* **2006**, *52* (1), 200–205.
3. Lindgren, A.; Emnéus, J.; Ruzgas, T.; Gorton, L.; Marko-Varga, G. Amperometric Detection of Phenols Using Peroxidase-Modified Graphite Electrodes. *Anal. Chim. Acta* **1997**, *347* (1–2), 51–62.
4. Bahadir, E. B.; Sezgintürk, M. K. Applications of Commercial Biosensors in Clinical, Food, Environmental, and Biothreat/Biowarfare Analyses. *Anal. Biochem.* **2015**, *478* (March), 107–120.
5. Rocchitta, G.; Spanu, A.; Babudieri, S.; Latte, G.; Madeddu, G.; Galleri, G.; Nuvoli, S.; Bagella, P.; Demartis, M. I.; Fiore, V.; Manetti, R.; Serra, P. A. Enzyme Biosensors for Biomedical Applications: Strategies for Safeguarding Analytical Performances in Biological Fluids. *Sensors (Switzerland)* **2016**, *16* (6).
6. Carrión, E. N.; Loas, A.; Patel, H. H.; Pelmuş, M.; Ramji, K.; Gorun, S. M. Fluoroalkyl Phthalocyanines: Bioinspired Catalytic Materials. *J. Porphyr. Phthalocyanines* **2018**, *22* (5), 371–397.
7. Al-Nu'Airat, J.; Dlugogorski, B. Z.; Gao, X.; Zeinali, N.; Skut, J.; Westmoreland, P. R.; Oluwoye, I.; Altarawneh, M. Reaction of Phenol with Singlet Oxygen. *Phys. Chem. Chem. Phys.* **2019**, *21* (1), 171–183.
8. Trashin, S.; Rahemi, V.; Ramji, K.; Neven, L.; Gorun, S. M.; De Wael, K. Singlet Oxygen-Based Electrosensing by Molecular Photosensitizers. *Nat. Commun.* **2017**, *8* (May), 1–10.
9. Neven, L.; Shanmugam, S. T.; Rahemi, V.; Trashin, S.; Sleegers, N.; Carrión, E. N.; Gorun, S. M.; De Wael, K. Optimized Photoelectrochemical Detection of Essential Drugs Bearing Phenolic Groups. *Anal. Chem.* **2019**, *91* (15), 9962–9969.
10. Rajh, T.; Chen, L. X.; Lukas, K.; Liu, T.; Thurnauer, M. C.; Tiede, D. M. Surface Restructuring of Nanoparticles: An Efficient Route for Ligand-Metal Oxide Crosstalk. *J. Phys. Chem. B* **2002**, *106* (41), 10543–10552.
11. Di Iorio, Y.; Parra, R.; Szaciłowski, K.; Grela, M. A. Alizarin Complexone: An Interesting Ligand for Designing TiO 2-Hybrid Nanostructures. *New J. Chem.* **2013**, *37* (4), 969–976.
12. Hayatsu, H. Cellulose Bearing Covalently Linked Copper Phthalocyanine Trisulphonate as an Adsorbent Selective for Polycyclic Compounds and Its Use in Studies of Environmental Mutagens and Carcinogens. *J. Chromatogr. A* **1992**, *597* (1–2), 37–56.
13. Ivo, Š.; Šafaříková, M. Copper Phthalocyanine Dye Immobilized on Magnetite Particles: An Efficient Adsorbent for Rapid Removal of Polycyclic Aromatic Compounds from Water Solutions and Suspensions. *Sep. Sci. Technol.* **1997**, *32* (14), 2385–2392.
14. Goldstein, B. P. Resistance to Rifampicin : A Review. *J. Antibiot. (Tokyo).* **2014**, *67* (9), 625–630.
15. Hughes, D.; Brandis, G. Rifampicin Resistance: Fitness Costs and the Significance of Compensatory Evolution. *Antibiotics*. 2013, pp 206–216.
16. Sanseverino, I.; Navarro, A.; Loos, R.; Marinov, D. State of the Art on the Contribution of Water to Antimicrobial Resistance. *JRC Tech. Rep.* **2018**.
17. Zhang, X.; Zhao, H.; Du, J.; Qu, Y.; Shen, C.; Tan, F.; Chen, J.; Quan, X. Occurrence, Removal, and Risk Assessment of Antibiotics in 12 Wastewater Treatment Plants from Dalian, China. *Environ. Sci. Pollut. Res.* **2017**, *24* (19), 16478–16487.
18. Escher, B. I.; Baumgartner, R.; Koller, M.; Treyer, K.; Lienert, J.; McArdell, C. S. Environmental Toxicology and Risk Assessment of Pharmaceuticals from Hospital Wastewater. *Water Res.* **2011**, *45* (1), 75–92.
19. Bench, B. A.; Beveridge, A.; Sharman, W. M.; Diebold, G. J.; Lier, J. E. Van; Gorun, S. M. Introduction of Bulky Perfluoroalkyl Groups at the Peryphery of Zinc Perfluorophthalocyanine. *Angew. Chem. Int. Ed. Engl.* **2002**, *41* (5), 747–750.
20. Jones, G.; Willett, P.; Glen, R. C.; Leach, A. R.; Taylor, R. Development and Validation of a Genetic Algorithm for Flexible Docking. *J. Mol. Biol.* **1997**.
21. Groom, C. R.; Bruno, I. J.; Lightfoot, M. P.; Ward, S. C. The Cambridge Structural Database. *Acta Crystallogr. Sect. B Struct. Sci. Cryst. Eng. Mater.* **2016**, *72* (2), 171–179.

22. Caudana, F.; Ermondi, G.; Vallaro, M.; Shalaeva, M.; Caron, G. Permeability Prediction for Zwitterions via Chromatographic Indexes and Classification into “certain” and “Uncertain.” *Future Med. Chem.* **2019**, *11* (13), 1553–1563.
23. Wicher, B.; Pyta, K.; Przybylski, P. Redetermination of Rifampicin Penta- Hydrate Revealing a Zwitterionic Form of the Antibiotic. **2012**, *287* (4), 209–212.
24. Li, J.; Zhu, M.; Rajamani, S.; Uversky, V. N.; Fink, A. L. Rifampicin Inhibits α-Synuclein Fibrillation and Disaggregates Fibrils. *Chem. Biol.* **2004**.
25. Garriga, D.; Headey, S.; Accurso, C.; Gunzburg, M.; Scanlon, M.; Coulibaly, F. Structural Basis for the Inhibition of Poxvirus Assembly by the Antibiotic Rifampicin. *Proc. Natl. Acad. Sci. U. S. A.* **2018**, *115* (33), 8424–8429.
26. Thapliyal, N.; Karpoormath, R. V; Goyal, R. N. Electroanalysis of Antitubercular Drugs in Pharmaceutical Dosage Forms and Biological Fluids: A Review. *Analytica Chimica Acta*. Elsevier B.V. 2015, pp 59–76.
27. Farokhi-Fard, A.; Golichenari, B.; Mohammadi Ghanbarlou, M.; Zanganeh, S.; Vaziri, F. Electroanalysis of Isoniazid and Rifampicin: Role of Nanomaterial Electrode Modifiers. *Biosens. Bioelectron.* **2019**, *146* (October), 111731.
28. Jindal, K. C.; Chaudhary, R. S.; Singla, A. K.; Gangwal, S. S.; Khanna, S. Effects of Buffers and PH on Rifampicin Stability. *Pharm. Ind.* **1995**, *57* (5), 420–422.
29. Balbão, M. S.; Bertucci, C.; Bergamaschi, M. M.; Queiroz, R. H. C.; Malfará, W. R.; Dreossi, S. A. C.; de Paula Mello, L.; Queiroz, M. E. C. Rifampicin Determination in Plasma by Stir Bar-Sorptive Extraction and Liquid Chromatography. *J. Pharm. Biomed. Anal.* **2010**, *51* (5), 1078–1083.
30. Asadpour-Zeynali, K.; Saeb, E. Simultaneous Spectrophotometric Determination of Rifampicin, Isoniazid and Pyrazinamide in a Single Step. *Iran. J. Pharm. Res.* **2016**, *15* (4), 713–723.
31. Kolmer, E. W. J. V. E.; Teulen, M. J. A.; Hombergh, E. C. A. Van Den; Erp, N. E. Van; Brake, L. H. M.; Aarnoutse, R. E. Determination of Protein-Unbound , Active Rifampicin in Serum by Ultra Fi Ltration and Ultra Performance Liquid Chromatography with UV Detection . A Method Suitable for Standard and High Doses of Rifampicin. *J. Chromatogr. B* **2018**, *1063* (July 2017), 42–49.
32. Allanson, A. L.; Cotton, M. M.; Tettey, J. N. A.; Boyter, A. C. Determination of Rifampicin in Human Plasma and Blood Spots by High Performance Liquid Chromatography with UV Detection : A Potential Method for Therapeutic Drug Monitoring. **2007**, *44*, 963–969.
33. Duarte, L. M.; Amorim, T. L.; Chellini, P. R.; Adriano, L. H. C.; de Oliveira, M. A. L. Sub-Minute Determination of Rifampicin and Isoniazid in Fixed Dose Combination Tablets by Capillary Zone Electrophoresis with Ultraviolet Absorption Detection. *J. Sep. Sci.* **2018**, *41* (24), 4533–4543.